Journal of Science and Technology – Smart Systems and Devices
Volume 36, Issue 2, May 2026, 074–081

Fast-Convergent Stabilization and Trajectory Tracking of a Two-Wheel Self-Balancing Robot on Sloped Terrain

Dinh Hieu Pham, Manh Linh Nguyen*

Hanoi University of Science and Technology, Ha Noi, Vietnam
**Corresponding author email: linh.nguyenmanh@hust.edu.vn*

Abstract

The Two-wheeled Balancing Robot system is increasingly demonstrating its importance in both research and practical applications. Ensuring stability and flexible mobility on complex terrains, particularly sloped surfaces, remains a significant challenge. To address this issue, the research presented in this paper first establishes a precise mathematical model for the robot system operating on a slope. Building upon this model, the paper proposes a novel control strategy based on an improved Hierarchical Sliding Mode Control (HSMC) technique incorporating a terminal sliding surface. The primary objective of this controller is to achieve extremely fast convergence speed, thereby simultaneously solving two key problems: maintaining stability at a fixed position on the slope and safely navigating the robot across the sloped area to reach a target destination in a 2D model. The research also provides an in-depth analysis of the system's operating point on the sloped terrain and offers a rigorous mathematical proof of the overall system's stability using Lyapunov stability theory. To validate the effectiveness, simulation results on the MATLAB/Simulink platform were conducted and directly compared with those of a conventional HSMC. The obtained results demonstrate that the proposed controller not only ensures higher stability but also exhibits superior responsiveness and performance in both assigned tasks.

Keywords: Hierarchical sliding mode control, terminal sliding surface, two-wheeled balancing robot, uprise.

1. Introduction

The two-wheeled balancing robot has long been an ideal research subject in the field of automatic control, owing to its inherently nonlinear, unstable dynamics and wide range of practical applications, from personal mobility devices to service robots [1–3]. While most previous studies have successfully addressed the problems of stability control and navigation for robots on flat surfaces, real-world environments often present non-ideal terrains. Among these, sloped surfaces represent a typical challenge. Maintaining balance and ensuring effective motion control on such terrain requires more advanced control strategies. This is due to the shift in the system's equilibrium point under the influence of gravity, which significantly complicates the model and the system's behavior.

Various control methods have been applied to this system, ranging from classical controllers like PID [4, 5] and LQR [5, 6] to more robust approaches such as Sliding Mode Control (SMC) [7, 8]. Among them, Hierarchical Sliding Mode Control (HSMC) has been employed by Chen *et al.* [9], demonstrating effectiveness in managing multivariate and unstable systems by decomposing the complex problem into sub-problems with subsidiary and main sliding surfaces. However, conventional HSMC controllers can suffer from limitations in the convergence speed to the equilibrium state, particularly in scenarios demanding high response speeds, such as operation on a slope. To overcome this limitation, integrating a Terminal Sliding Surface (TSS) [10] into the traditional control structure has emerged as a promising solution, offering the potential for finite-time convergence due to its fast convergence characteristics.

The current state of the art primarily addresses controlling this model on horizontal planes or focuses solely on stabilization at a desired position. For instance, in [11], Muñoz-Hernandez and colleagues utilized Active Disturbance Rejection Control (ADRC) on a practical model and demonstrated the system's ability to balance the inverted pendulum, but did not address other core issues such as traversal across flat surfaces or slope climbing. Other studies [7, 12] have tackled the aspect of navigation by controlling the robot to track a predefined trajectory, but only in flat environments. Therefore, building upon this research is crucial to enhance the feasibility of controlling the model in classic environments like ascending or descending slopes, ensuring its operability in a wider range of scenarios.

It is important to emphasize that although this research is based on a 2D model with a single representative wheel and an inverted pendulum structure, it accurately captures the core dynamic behavior of a 3D robot in a slope scenario. In practice, for a full two-wheeled robot to stably ascend a slope, both wheels must maintain contact with the sloped surface simultaneously. This implies that the cross-section along the direction of travel for the 3D problem is precisely the

p-ISSN 3093-3285
e-ISSN 3093-3315
https://doi.org/10.51316/jst.190.ssad.2026.36.2.9
Received: Nov 28, 2025; Revised: Dec 23, 2026;
Accepted: Jan 6, 2026; Online: Jan 16, 2026

2D model under consideration. Consequently, analysis based on the 2D model not only simplifies the problem but also maintains dynamical rigor, providing crucial insights that can be applied to the 3D model.

To address the aforementioned challenges, this paper focuses on developing a hybrid controller that combines the structural management advantages of HSMC with the superior convergence capabilities of the Terminal Sliding Surface. The specific objectives of this research are:

1) To establish a precise mathematical model using the Lagrange method for the two-wheeled balancing robot operating on a sloped surface, including an analysis of the system's new operating point.
2) To design a hierarchical sliding mode controller utilizing a terminal sliding surface (HSMC-TSS) to stabilize the robot at a fixed position on the slope and safely navigate the robot across a sloped section to reach a target destination within the 2D model framework.

The remainder of this paper is organized as follows: Section 2 presents the dynamic modeling of the robot on a slope. Section 3 introduces the design of the proposed HSMC-TSS controller and its stability analysis. Section 4 presents and discusses simulation results. Finally, Section 5 provides conclusions and suggests future research directions.

2. Mathematical Model

The 2WBR model moving on a slope constructed on a 2D plane is illustrated in Fig. 1. Let x denote the translational motion state along the direction of travel. The computational coordinate frame Oij is placed at the base of the slope such that its horizontal axis corresponds to the translational motion direction of the model, while the slope has a constant inclination angle φ. The deviation between the inverted pendulum angle and the vertical direction is defined as θ.

The parameters and symbols of the model are presented in Table 1.

The coordinates based on the Oij frame of the inverted pendulum are:

$$\begin{aligned} x_P &= x + l\sin(\theta+\varphi) \\ y_P &= l\cos(\theta+\varphi) \end{aligned} \tag{1}$$

The vector representing the position of the inverted pendulum $\vec{r}_P$ is:

$$\vec{r}_P = [x + l\sin(\theta+\varphi)]\vec{i} + [l\cos(\theta+\varphi)]\vec{j} \tag{2}$$

From the position vector in (2), by differentiating with respect to time, the velocity of the inverted pendulum is obtained as:

$$\vec{v}_P = [\dot{x} + \dot{\theta} l\cos(\theta+\varphi)]\vec{i} - [\dot{\theta} l\sin(\theta+\varphi)]\vec{j} \tag{3}$$

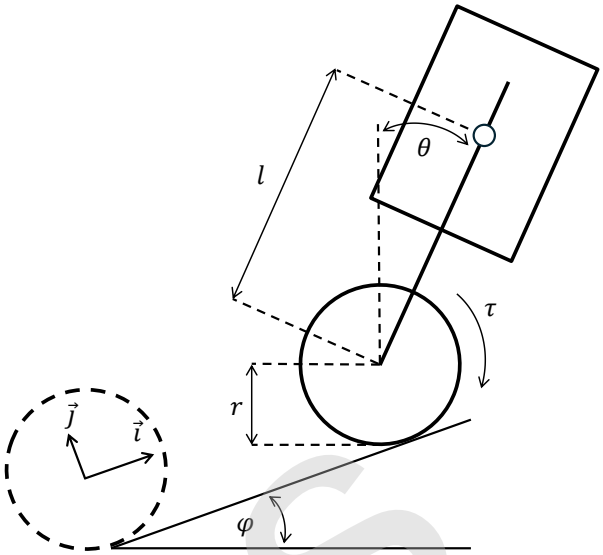

Fig. 1. Uprise model in 2D

Table 1. Model parameters

Description	Symbol	Unit
Mass of wheel	m_W	kg
Inertial of wheel	I_W	$kg.m^2$
Mass of inverted pendulum	m_P	kg
Inertial of inverted pendulum	I_P	$kg.m^2$
Radius of wheel	r	m
Length of inverted pendulum	l	m
Gravitational acceleration	g	m/s^2
Friction coefficient	c_f	

The kinetic energy of the model consists of the sum of translational and rotational kinetic energies. The translational kinetic energy is calculated as:

$$\begin{aligned} T_{trans} &= \frac{1}{2} v_P^T m_P v_P + \frac{1}{2} m_W \dot{x}^2 \\ &= \frac{1}{2} m_P [\dot{x} + \dot{\theta} l\cos(\theta+\varphi)]^2 \\ &\quad + \frac{1}{2} m_P [\dot{\theta} l\sin(\theta+\varphi)]^2 + \frac{1}{2} m_W \dot{x}^2 \end{aligned} \tag{4}$$

and the sum of rotational kinetic energy in the model is defined as:

$$T_{rot} = \frac{1}{2} I_P \dot{\theta}^2 + \frac{1}{2} I_W \left(\frac{\dot{x}}{r}\right)^2 \tag{5}$$

With the reference potential set at the base of the slope, the potential energy of the model is:

$$V = m_P g(l\cos\theta + x\sin\varphi) + m_W g x\sin\varphi \tag{6}$$

The Lagrangian is defined as the difference between the kinetic energy and the potential energy.

$$L = T_{trans} + T_{rot} - V \tag{7}$$

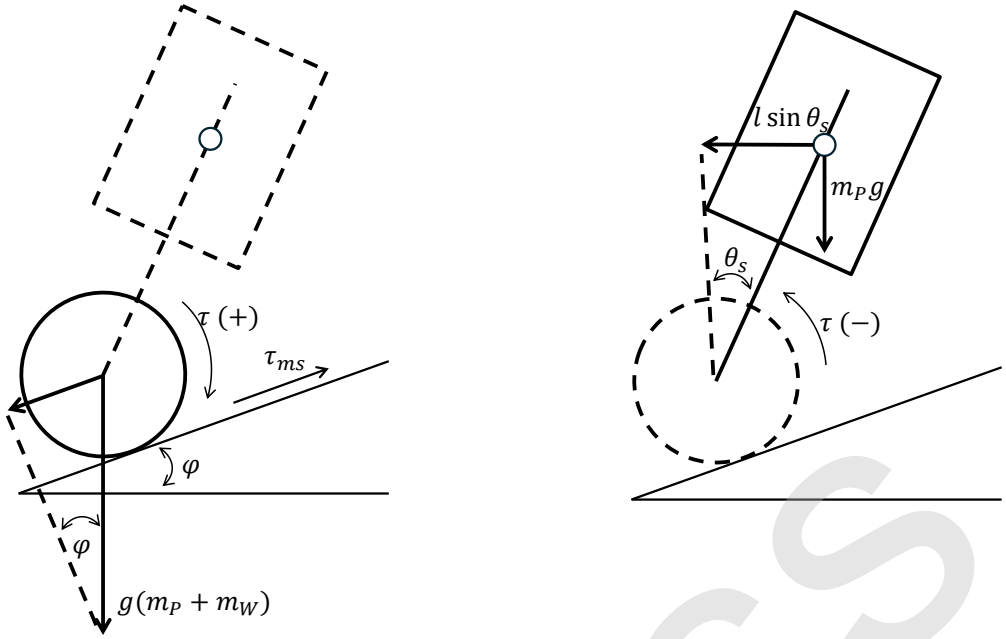

Fig. 2. The external forces acting on the model when it is leaning on a slope

To model the system, the Euler-Lagrange equation is formulated with two components $q = [x \quad \theta] = [q_x \quad q_\theta]$:

$$\frac{d}{dt}\left(\frac{\partial L}{\partial \dot{q}_i}\right) - \frac{\partial L}{\partial q_i} = Q_i \qquad i = \{x;\theta\} \tag{8}$$

where Q_i are the generalized forces associated with external forces (the friction between the drive shafts and the friction between the wheels and the slope) and the torque of the wheels acting on the model, given by:

$$\begin{aligned} Q_x &= \frac{1}{r}(\tau + \tau_{ms}) \\ Q_\theta &= -\tau - \tau_{ms} \end{aligned} \tag{9}$$

After solving the Euler-Lagrange equations, the system of equations is obtained as follows:

$$\begin{aligned} &a\ddot{x} + b\ddot{\theta} - m_P l \sin(\theta+\varphi)\dot{\theta}^2 \\ &\qquad + g(m_P + m_W)\sin\varphi = \frac{1}{r}(\tau + \tau_{ms}) \\ &b\ddot{x} + c\ddot{\theta} - m_P l g \sin\theta = -\tau - \tau_{ms} \end{aligned} \tag{10}$$

where $a = m_W + m_P + \frac{I_w}{r^2}$, $b = m_P l \cos(\theta+\varphi)$, and $c = I_P + m_P l^2$.

The above equations can be expressed in matrix form as:

$$M\ddot{q} + C\dot{q} + H\dot{q} + G = B\tau \tag{11}$$

where

$$\begin{aligned} M &= \begin{bmatrix} a & b \\ b & c \end{bmatrix}; \qquad C = \begin{bmatrix} 0 & m_P l \sin(\theta+\varphi)\dot{\theta} \\ 0 & 0 \end{bmatrix}; \\ H &= \begin{bmatrix} -\frac{1}{r}\tau_{ms} \\ \tau_{ms} \end{bmatrix}; \qquad B = \begin{bmatrix} \frac{1}{r} \\ -1 \end{bmatrix}; \\ G &= \begin{bmatrix} -g(m_P + m_W)\sin\varphi \\ -m_P l g \sin\theta \end{bmatrix}. \end{aligned} \tag{12}$$

and c_f denotes the coefficient of friction, so τ_{ms} is defined as $\tau_{ms} = c_f\left(\frac{\dot{x}}{r} - \dot{\theta}\right)$.

In the model, when the system reaches an equilibrium state, the acceleration and velocity states satisfy $\ddot{x} = 0$, $\dot{x} = 0$, $\ddot{\theta} = 0$, $\dot{\theta} = 0$, and the external disturbance $\tau_{ms} = 0$. In this condition, the system is described by:

$$\begin{aligned} &g(m_P + m_W)\sin\varphi = \frac{1}{r}\tau \\ &-m_P l g \sin\theta_s = -\tau \end{aligned} \tag{13}$$

where θ_s is the equilibrium angle when climbing the slope. From the system of (13), the equilibrium angle can be determined as:

$$\theta_s = \arcsin\frac{r\sin\varphi(m_P + m_W)}{m_P l} \tag{14}$$

This result is consistent with real-world behavior: when the robot remains stationary on a slope, the inverted pendulum must tilt by an angle θ_s away from the vertical position to generate a compensating wheel torque that balances the gravitational component pulling the system downhill. This phenomenon is illustrated more clearly in Fig. 2.

Thus, for a typical model on a horizontal plane, the desired tilt angle θ_s is 0 (rad) relative to the vertical direction. However, in the case of operation on a slope, the desired angle θ_s is determined by the expression above.

3. Control Design

With the control structure described in Fig. 3, the predefined reference states include the position and the tilt angle, which is computed based on the slope.

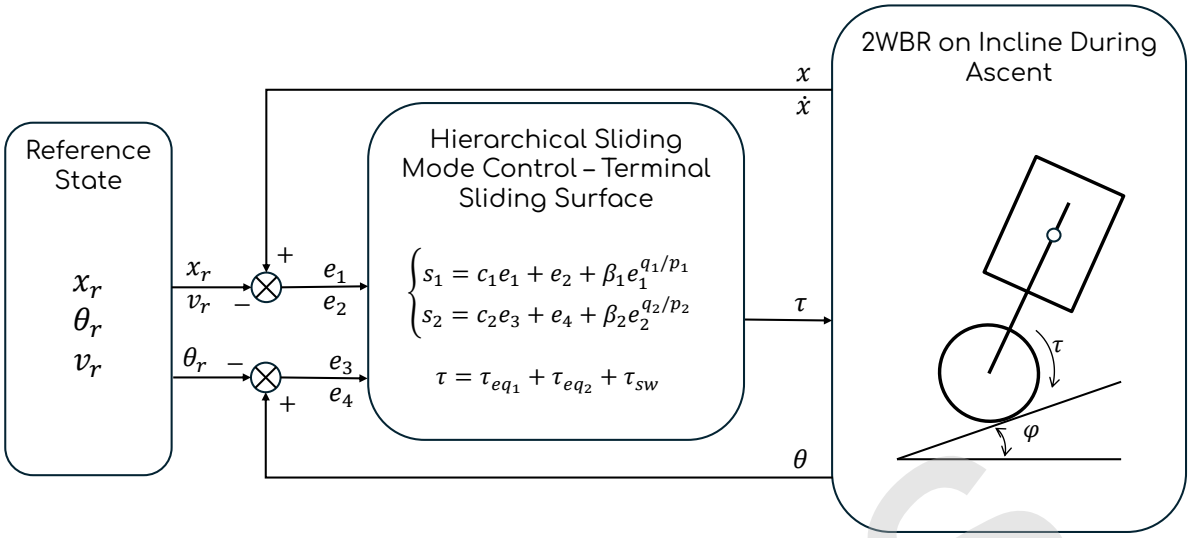

Fig. 3. Control structure

Normally, on a horizontal plane, the desired tilt angle θ is always equal to 0. However, in the case of operation on a slope, the desired tilt angle corresponds to a different value, as presented in (14), in order to generate the necessary moment that produces the appropriate θ for stabilizing the system at the specified position.

3.1. Terminal Sliding Surface

With a general system, to achieve fast convergence of the system, the terminal sliding surface is designed as:

$$s = \dot{y} + \alpha y + \beta y^{q/p} \tag{15}$$

where $y \in \mathscr{R}$ is a state variable of the system, α and β are positive constants, p and q ($p > q$) are positive odd integers.

When the state of model reaches the sliding surface ($s = 0$), the dynamics are governed by:

$$\dot{y} = -\alpha y - \beta y^{q/p} \tag{16}$$

To derive the finite convergence time from an initial state $y(0) \neq 0$ to $y = 0$, we solve this differential equation using separation of variables:

$$\begin{aligned} &\frac{dy}{dt} = -\alpha y - \beta y^{q/p} \\ \Rightarrow \quad &\frac{dy}{\alpha y + \beta y^{q/p}} = -dt \end{aligned} \tag{17}$$

Rewriting the left side:

$$\frac{dy}{y^{q/p}(\alpha y^{(p-q)/p} + \beta)} = -dt \tag{18}$$

Let $z = y^{(p-q)/p}$, then:

$$\begin{aligned} &dz = \frac{p-q}{p} y^{-q/p} dy \\ \Rightarrow \quad &\frac{dy}{y^{q/p}} = \frac{p}{p-q} dz \end{aligned} \tag{19}$$

Substituting into the equation:

$$\frac{p}{p-q} \cdot \frac{dz}{\alpha z + \beta} = -dt \tag{20}$$

Integrating both sides from the initial state to the equilibrium:

$$\int_{z(0)}^{0} \frac{p}{p-q} \cdot \frac{du}{\alpha z + \beta} = -\int_0^{t_s} dt \tag{21}$$

where $z(0) = y(0)^{(p-q)/p}$ and t_s is the finite convergence time. Solving the integrals:

$$\frac{p}{\alpha(p-q)} [\ln(\alpha z + \beta)]_{z(0)}^{0} = -t_s \tag{22}$$

After applying the integration limits:

$$\frac{p}{\alpha(p-q)} \left[\ln(\beta) - \ln(\alpha y(0)^{(p-q)/p} + \beta) \right] = -t_s \tag{23}$$

Finally, solving for t_s:

$$t_s = \frac{p}{\alpha(p-q)} \ln \frac{\alpha y(0)^{(p-q)/p} + \beta}{\beta} \tag{24}$$

Equation 24 demonstrates that the system achieves convergence to the equilibrium point in finite time, a significant advantage over conventional linear sliding surfaces, which only guarantee asymptotic convergence. This property is particularly important for systems requiring fast response and high precision.

3.2. Hierarchical Sliding Mode Control

Considering (11), the matrix M is the mass matrix and therefore invertible. Accordingly, both sides of this equation can be multiplied by the inverse of M. This allows the system to be written in a form where the state accelerations are isolated, making computations more

straightforward.

$$\begin{cases} \dot{x}_1 = x_2 \\ \dot{x}_2 = f_1 + g_1\tau \\ \dot{x}_3 = x_4 \\ \dot{x}_4 = f_2 + g_2\tau \end{cases} \tag{25}$$

where f_i, g_i $(i = 1,2)$ are the nonlinear functions in the model. Let X and u denote the overall state of the system and the input signal, respectively. The HSMC controller is designed to control the states including: position (x), velocity $(\dot{x})$, tilt angle (θ), and angular velocity $(\dot{\theta})$. The tracking errors of the output states relative to the desired values are defined as:

$$\begin{cases} e_1 = x - x_d \\ e_2 = \dot{x} - \dot{x}_d \\ e_3 = \theta - \theta_d \\ e_4 = \dot{\theta} - \dot{\theta}_d \end{cases} \tag{26}$$

The system sliding surfaces are constructed based on the Terminal Sliding Surface, defined as:

$$\begin{cases} s_1 = e_2 + \alpha_1 e_1 + \beta_1 e_1^{(q_1/p_1)} \\ s_2 = e_4 + \alpha_2 e_3 + \beta_2 e_3^{(q_2/p_2)} \end{cases} \tag{27}$$

where $\alpha_1, \alpha_2, \beta_1, \beta_2$ are positive constants, and q_1, p_1, p_2, q_2 are positive odd integers. The hierarchical sliding surface is constructed based on these two surfaces:

$$S = k_1 s_1 + k_2 s_2 \tag{28}$$

To calculate the equivalent control signal τ_{eq_1}, consider the sliding surface $\dot{s}_1 = 0$:

$$\tau_{eq_1} = -\frac{f_1 + \alpha_1 \dot{e}_1 + \frac{q_1}{p_1}\beta_1 e_1^{(q_1/p_1 - 1)}\dot{e}_1 - \ddot{x}_d}{g_1} \tag{29}$$

Similarly:

$$\tau_{eq_2} = -\frac{f_2 + \alpha_2 \dot{e}_3 + \frac{q_2}{p_2}\beta_2 e_3^{(q_2/p_2 - 1)}\dot{e}_3 - \ddot{\theta}_d}{g_2} \tag{30}$$

The HSMC control signal to achieve the desired states is given by:

$$\tau = \tau_{eq_1} + \tau_{eq_2} + \tau_{sw} \tag{31}$$

where τ_{sw} is expressed as:

$$\tau_{sw} = -\frac{k_1 g_1 \tau_{eq_2} + k_2 g_2 \tau_{eq_1} + \eta\,\mathrm{sign}(S) + \varepsilon S}{k_1 g_1 + k_2 g_2} \tag{32}$$

For sliding mode controllers, a major drawback is chattering, which is a phenomenon that causes the control signal to switch continuously at high frequencies due to the sign function, leading to wear and potential damage to the motor. Therefore, the hyperbolic tangent (tanh) function is often employed to mitigate this effect. Accordingly, τ_{sw} is rewritten as:

$$\tau_{sw} = -\frac{k_1 g_1 \tau_{eq_2} + k_2 g_2 \tau_{eq_1} + \eta \tanh(S) + \varepsilon S}{k_1 g_1 + k_2 g_2} \tag{33}$$

Here, η and ε are positive control parameters. To prove stability, the candidate Lyapunov function is chosen as:

$$V = \frac{1}{2}S^2 \tag{34}$$

Then, its derivative is:

$$\begin{aligned} \dot{V} &= S\dot{S} = S(k_1\dot{s}_1 + k_2\dot{s}_2) \\ &= S[k_1(\dot{e}_2 + \alpha_1\dot{e}_1 + \frac{q_1}{p_1}\beta_1 e_1^{(q_1/p_1-1)}\dot{e}_1) \\ &+ k_2(\dot{e}_4 + \alpha_2\dot{e}_3 + \frac{q_2}{p_2}\beta_2 e_3^{(q_2/p_2-1)}\dot{e}_3)] \\ &= S[k_1(f_1 + g_1\tau + \alpha_1\dot{e}_1 + \frac{q_1}{p_1}\beta_1 e_1^{(q_1/p_1-1)}\dot{e}_1 - \ddot{x}_d) \\ &\quad + k_2(f_2 + g_2\tau + \alpha_2\dot{e}_3 + \frac{q_2}{p_2}\beta_2 e_3^{(q_2/p_2-1)}\dot{e}_3 - \ddot{\theta}_d)] \\ &= S[k_1(f_1 + g_1(\tau_{eq_1} + \tau_{eq_2} + \tau_{sw}) + \alpha_1\dot{e}_1 \\ &\quad + k_2(f_2 + g_2(\tau_{eq_1} + \tau_{eq_2} + \tau_{sw}) + \alpha_2\dot{e}_3 \\ &\quad + \frac{q_1}{p_1}\beta_1 e_1^{(q_1/p_1-1)}\dot{e}_1 - \ddot{x}_d) + \frac{q_2}{p_2}\beta_2 e_3^{(q_2/p_2-1)}\dot{e}_3 - \ddot{\theta}_d)] \\ &= S[k_1 g_1(\tau_{eq_2} + \tau_{sw}) + k_2 g_2(\tau_{eq_1} + \tau_{sw})] \\ &= S[(k_1 g_1 + k_2 g_2)\tau_{sw} + k_1 g_1 \tau_{eq_2} + k_2 g_2 \tau_{eq_1}] \\ &= S[-\eta\tanh(S) - \varepsilon S] \\ &= -\eta\tanh(S)S - \varepsilon S^2 \end{aligned} \tag{35}$$

Because $\tanh(S)S \geq 0$, it is clear that $\dot{V} \leq 0$. Therefore, the system is asymptotic stability in the sense of Lyapunov. This implies that the large sliding surface S converges to 0, which means that both s_1 and s_2 converge to 0. Consequently, the controlled states x, $\dot{x}$, θ, and $\dot{\theta}$ are regulated as desired.

4. Simulation Results

The parameters of the model are given as follows: $m_W = 1.551\ kg, m_P = 1.6\ kg, I_W = 0.005\ kg.m^2, I_P = 0.027\ kg.m^2, r = 0.08\ m, l = 0.13\ m, g = 9.81\ m/s^2$, $c_f = 0.07$.

The control parameters used for the simulation are: $\alpha_1 = 2.5$, $\alpha_2 = 6$, $\beta_1 = 0.015, \beta_2 = 0.015$, $p_1 = p_2 = 9$, $q_1 = q_2 = 13$, $k_1 = 17, k_2 = 3, \eta = 3, \varepsilon = 1$.

4.1. Stability

To verify the feasibility of the proposed controller, simulation in the case of stabilizing at a desired position is essential. In this scenario, the simulation is compared with HSMC but using a conventional sliding surface of

the form $s = \dot{y} + \lambda y$, where y is a general state variable of the system, λ is positive constant. The initial states of the model are: $x = 0\ (m), \dot{x} = 0\ (m/s), \theta = 0.2\ (rad), \dot{\theta} = 0\ (rad/s)$. The desired position is to move 1 m, meaning that $x_d = 1\ (m)$, remain stable at that location.

Figure 4 illustrates the responses of the position and the tilt angle of the model. The response corresponding to the proposed controller in this scenario is denoted with the subscript TSS, the response of the conventional HSMC controller is denoted with SS, and the desired state is marked with the subscript d. Since the friction coefficient is not easy to measure accurately in practice, the terms τ_{ms} related to c_f are treated as uncertainties in the model. Furthermore, a pulse-type disturbance with an amplitude of 2 Nm is applied to the system during the time interval from 5.5s to 6s in order to evaluate the robustness of the model.

The results show that the proposed controller with the terminal sliding surface enables the system to respond faster, achieving convergence in approximately 2s, compared to 3s for the conventional HSMC with a standard sliding surface. Meanwhile, the nature of this model involves coupled translational motion and the tilt angle of the inverted pendulum. Therefore, overshoot is intrinsic and cannot be avoided. Given the initial conditions and the objective of achieving rapid stabilization, there is an inherent trade-off between overshoot and response time. As observed during the transient phase from 0s to 4s, the model exhibits a larger overshoot under the proposed controller compared with the conventional HSMC. However, when an external disturbance is applied, the faster response enabled by the terminal sliding surface becomes evident, as the settling time required to return to the equilibrium position is shorter than that of the conventional sliding surface. Moreover, during this phase, not only is the recovery time reduced, but the deviation is also smaller ($-0.17rad$ compared with $-0.32rad$ in response of tilt state). These results further demonstrate that, with the objective of achieving a faster response, the disturbance rejection capability is also improved by driving the system back to the equilibrium position as quickly as possible.

The control torque is shown in Fig. 5. When the system reaches stability, the tilt angle θ is not positioned at zero; therefore, the control signal always maintains a nonzero value to sustain control.

4.2. Tracking Uprise

Using the same proposed controller and model as above, this simulation scenario controls the model's position over time to examine the state responses. A white-noise measurement noise is introduced into the feedback signal of the controller for the tilt state and the model still contains an unknown friction coefficient c_f. The model is required to move along flat, ascending, and descending segments. The terrain profile is illustrated in Fig. 6.

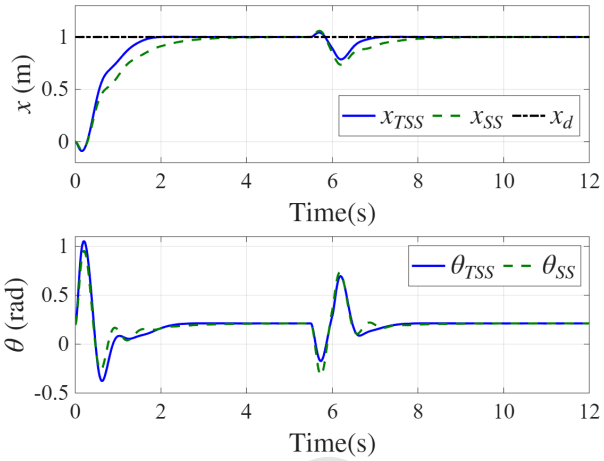

Fig. 4. State response

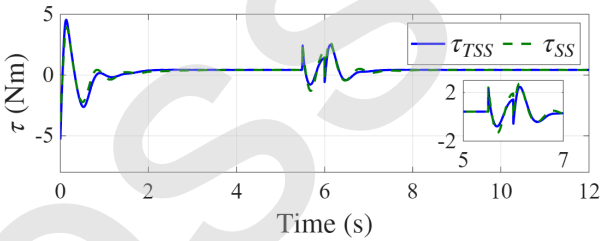

Fig. 5. Control signal

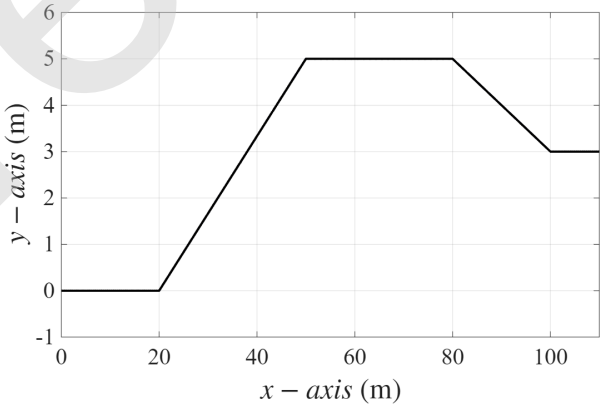

Fig. 6. Cross-section of the terrain

The simulation scenario features a segmented terrain profile designed to comprehensively evaluate the robot's performance. The path begins with a flat segment from the starting point at $0m$ to approximately $20m$, allowing for initial stabilization. It is followed by an ascending slope that commences at around $20m$ and concludes at roughly $50m$, testing the robot's climbing capability and stability on an incline. Upon reaching the top, the robot traverses a second flat section from about $50m$ to $80m$, validating its stability on a leveled surface after a climb. The path then transitions to a descending slope from approximately $80m$ to $100m$, challenging its control during downhill motion. Finally, the terrain levels out into a concluding flat segment from $100m$ onward, assessing the robot's ability to regain and maintain equilibrium after navigating the complete slope sequence.

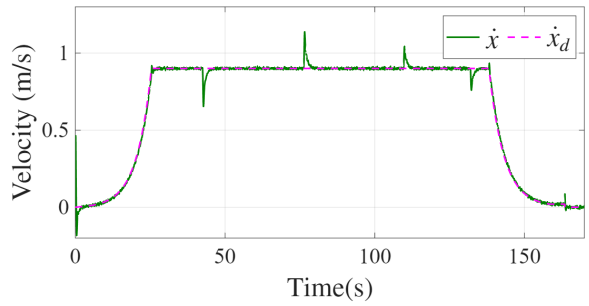

Fig. 7. Velocity response

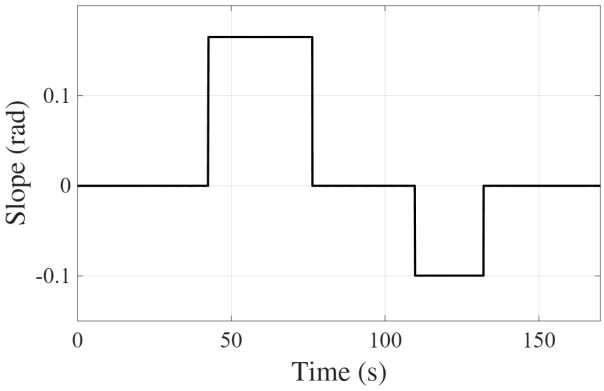

Fig. 8. Slope profile

The feasible trajectory is achieved through velocity-based control. Fig. 7 illustrates the reference velocity and the actual velocity response of the model. Observations indicate that the velocity response exhibits sudden increases and decreases, which occur as the model approaches or leaves sloped segments during motion. Furthermore, the measured velocity of the model exhibits small high-frequency oscillations due to the measurement noise that has been introduced. Therefore, the variation in terrain slope over time is depicted in Fig. 8 to further clarify this relationship.

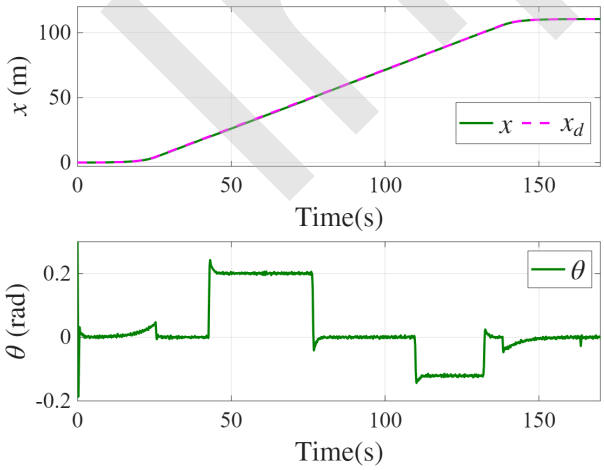

Fig. 9. State response

The state response of the model is illustrated in Fig. 9. In terms of position tracking, the results demonstrate accurate and satisfactory performance. Meanwhile, the tilt angle θ varies according to the terrain during movement. Specifically, on flat terrain, the inverted pendulum's deviation oscillates around a value of $0rad$. On the other hand, when moving on sloped terrain, this tilt angle adjusts to accommodate the motion. When measurement noise is introduced into the feedback loop of the controller, it also affects the system response. The robustness of the sliding mode controller is demonstrated by these results, although this type of measurement noise cannot be completely eliminated. Since the position tracking response is highly accurate, Fig. 10 depicts the deviation between the actual state response and the desired value. The results indicate a maximum deviation of only $0.2m$ when traversing slopes, with this error becoming more pronounced as the slope steepness increases.

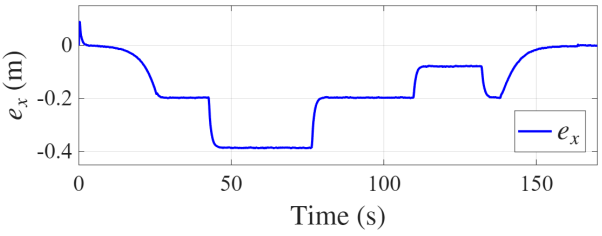

Fig. 10. Error of translational state

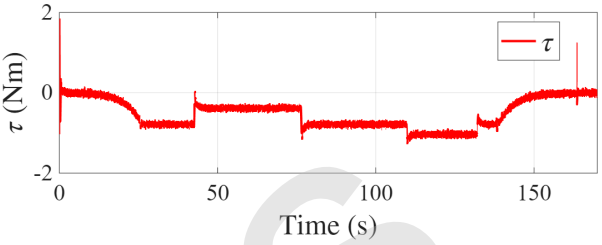

Fig. 11. Control signal

The control signal, presented in Fig. 11, exhibits a similar pattern to the descriptions above during operation. The proposed controller, fundamentally derived from sliding mode control, inherently suffers from the chattering phenomenon. However, the control signal has been significantly mitigated by replacing the sign function in the controller with another function that captures the sign of the sliding surface, a hyperbolic function. The phenomenon observed in the results shown in the figure is mainly not caused by the chattering associated with the hyperbolic function, but rather by measurement noise, and the controller generates control signals to counteract these variations.

5. Conclusion

In conclusion, this paper has successfully developed and validated a hierarchical sliding mode control strategy integrated with a terminal sliding surface for two-wheeled balancing robots navigating sloped terrains. The proposed HSMC-TSS controller demonstrates superior performance in achieving both precise position tracking and effective balance maintenance across various terrain segments, including ascending, descending, and flat surfaces,

with significantly faster convergence compared to conventional HSMC. While the controller shows promising robustness in the tested scenarios, its performance under more significant external disturbances and model uncertainties requires further investigation. Future research will focus on implementing this control strategy on a physical robotic platform to validate its practical efficacy, alongside enhancing its robustness to handle broader operational conditions and more challenging environmental factors.

References

[1] Z. Han, J. Long, W. Wang, and L. Wang, Adaptive tracking control of two-wheeled mobile robots under denial-of-service attacks, ISA Transactions, vol. 141, pp. 365–376, 2023.

[2] M. R. Islam, M. R. T. Hossain, and S. C. Banik, Synchronizing of stabilizing platform mounted on a two-wheeled robot, Journal of Robotics and Control (JRC), vol. 2, no. 6, pp. 552–558, 2021.

[3] A. Aldhalemi, A. Chlaihawi, and A. Al-Ghanimi, Design and implementation of a remotely controlled two-wheel self-balancing robot, in IOP Conference Series: Materials Science and Engineering, 2021, pp. 012132.

[4] V. Mudeng, B. Hassanah, Y. T. K. Priyanto, and O. Saputra, Design and simulation of two-wheeled balancing mobile robot with PID controller, International Journal of Sustainable Transportation Technology, vol. 3, no. 1, pp. 12–19, 2020.

[5] Y. Olmez, G. O. Koca, and Z. H. Akpolat, Clonal selection algorithm based control for two-wheeled self-balancing mobile robot, Simulation Modelling Practice and Theory, vol. 118, pp. 102552, 2022.

[6] L. M. M. Thwin and Y. Chan, Application of LQR control for two-wheel self-balancing robot, Journal of Myanmar Academy of Arts and Science, vol. 28, no. 2, pp. 263–272, 2020.

[7] N. Esmaeili, A. Alfi, and H. Khosravi, Balancing and trajectory tracking of two-wheeled mobile robot using backstepping sliding mode control: design and experiments, Journal of Intelligent & Robotic Systems, vol. 87, no. 3, pp. 601–613, 2017.

[8] M. Doğan and Ü. Önen, Trajectory tracking control of a two wheeled self-balancing robot by using sliding mode control, Konya Journal of Engineering Sciences, vol. 12, no. 3, pp. 652–670, 2024.

[9] L. Chen, H. Wang, Y. Huang, Z. Ping, M. Yu, X. Zheng, M. Ye, and Y. Hu, Robust hierarchical sliding mode control of a two-wheeled self-balancing vehicle using perturbation estimation, Mechanical Systems and Signal Processing, vol. 139, pp. 106584, 2020.

[10] H. Benbouhenni, I. Colak, and N. Bizon, Application of genetic algorithm and terminal sliding surface to improve the effectiveness of the proportional–integral controller for the direct power control of the induction generator power system, Engineering Applications of Artificial Intelligence, vol. 125, pp. 106681, 2023.

[11] G. A. Muñoz-Hernandez, J. Díaz-Téllez, J. Estevez-Carreon, and R. S. García-Ramírez, ADRC attitude controller based on ROS for a two-wheeled self-balancing mobile robot, IEEE Access, vol. 11, pp. 94636–94646, 2023. https://doi.org/10.1109/ACCESS.2023.3308948.

[12] Á. Odry, R. Fullér, I. J. Rudas, and P. Odry, Fuzzy control of self-balancing robots: A control laboratory project, Computer Applications in Engineering Education, vol. 28, no. 3, pp. 512–535, 2020.